Whistler Waves above the Lower Hybrid Frequency in the Ionosphere and their Counterparts in the Magnetosphere

Zhiyang Xia[1], Lunjin Chen[1], Richard B. Horne[2], Jacob Bortnik[3]

Zhiyang Xia, Department of Physics, University of Texas at Dallas, Richardson, Texas, USA 75080 (Zhiyang.Xia@utdallas.edu)

[1]Department of Physics, University of Texas at Dallas, Richardson, Texas, USA

[2]British Antarctic Survey, Cambridge, UK

[3]Department of Atmospheric and Oceanic Sciences, UCLA, Los Angeles, CA, USA

In this study, we report the statistical properties of whistler mode low hybrid (LH) emissions in the ionosphere, which have structureless spectra with a lower frequency boundary that matches the variation of the local lower hybrid resonance frequency f_{LHR}. A potential source for the low hybrid emissions is identified as the high-frequency plasmaspheric hiss (HFPH) in the magnetosphere. We use DEMETER and Van Allen Probes data to perform a statistical study of the wave power distribution of the LH emissions and HFPH. Both LH and HFPH emissions show a similar frequency range, a similar invariant magnetic latitude range, and have similar trends in magnetic local time (MLT) (stronger wave intensity on the dayside) and in the AE index (stronger wave intensity for higher AE condition). A ray tracing simulation is also performed to demonstrate the propagation of HFPH waves from the magnetosphere into the ionosphere as LH waves.

1. Introduction

Whistler mode waves are right hand circularly polarized electromagnetic waves in the very low frequency (VLF) range and play very important roles in the loss of high energy electrons via cyclotron resonance and Landau resonance [e.g., *Inan and Tkalcevic*, 1982; *Inan and Bell*, 1991; *Bell*, 1984, 1986; *Shklyar and Matsumoto*, 2009; *Artemyev et al.*, 2013]. Typical types of whistler mode waves, such as chorus waves, plasmaspheric hiss, lightning generated whistlers and whistlers that originate from ground-based transmitters, can often be observed in the Earth's ionosphere and magnetosphere. Whistler mode waves can propagate through the region that contains the Earth's ionosphere and magnetosphere, and the propagation process includes refraction, guiding, scattering and reflection under the control of the plasma density and background magnetic field. When the local lower hybrid resonance frequency f_{LHR} is close to the wave frequency, a whistler mode wave can completely reverse its direction, which is known as magnetospheric reflection [*Chum and Santolík*, 2005; *Jiřiček et al.*, 2001; *Lyons and Thorne*, 1970; *Shklyar et al.*, 2004; *Xu et al.*, 2020].

In the magnetosphere, the plasmaspheric hiss is usually observed as incoherent, structureless emissions with a wide frequency band from ∼100 Hz to 2 kHz [*Thorne et al.*, 1973; *Ni et al.*, 2013, 2014; *Yu et al.*, 2017; *Su et al.*, 2018]. The main sources of hiss wave generation include local excitation by electron injections [*Li et al.*, 2013; *Shi et al.*, 2017; *He et al.*, 2019], chorus propagation from the region outside of the plasmapause into the plasmasphere [*Bortnik et al.*, 2008, 2009; *Chen et al.*, 2009, 2012; *Yue et al.*, 2017] and lightning-generated whistlers [*Bortnik et al.*, 2003; *Draganov et al.*, 1992; *Meredith et al.*, 2006; *Sonwalkar and Inan*, 1989]. The high-frequency plasmaspheric hiss (HFPH) is a kind of high-frequency hiss wave with a frequency of up to 10 kHz that can be locally excited by substorm-injected electrons with an energy of approximately 1 keV [*He et al.*, 2019]. A statistical study from the Van Allen Probes' observations [*He et al.*, 2020] indicates that the HFPH intensity is stronger from the predawn to dusk region and under geomagnetically active conditions compare to quiet times. Additionally, the statistical spectra show that the frequency of HFPH increases with the background magnetic field and that the power of the HFPH is concentrated between 0.1 and 0.5 f_{ce}.

Lightning-generated whistlers (LGWs) are often observed in both the magnetosphere and the ionosphere and are generated by electromagnetic waves that are produced by lightning strokes leaking from the Earth-ionosphere waveguide and propagating through the ionosphere into the magnetosphere. The contribution of the LGWs to the wave intensity in the inner magnetosphere has been studied from the observations of DEMETER, the Van Allen Probes satellites and the World Wide Lightning Location Network (WWLLN). Previous studies show that the LGW wave intensity is stronger on the nightside than on the dayside, and is highly controlled by lightning activity on the ground [*Němec et al.*, 2010; *Záhlava et al.*, 2018b, 2019; *Zheng et al.*, 2016; *Ripoll et al.*, 2020; *Green et al.*, 2020].

In this study, we use the measurement from the Detection of Electromagnetic Emissions Transmitted from Earthquake Regions (DEMETER) satellite to provide observations of strong VLF emissions with frequencies that substantially exceed the local lower hybrid resonance frequency (f_{LHR}) at the topside of the ionosphere. The possibility that LGW is the source of the LH emission is excluded due to the different wave spectral structures and the wave power dependence on the local time and AE index. To determine the source of these LH emissions, using the measurements of DEMETER and Van Allen Probes, we statistically study the wave power distribution versus frequency and the magnetic latitude for both LH emissions in the ionosphere and the HFPH wave in the magnetosphere and find satisfactory agreements of these two wave power distributions in terms of the frequency range, latitude range, MLT dependence and AE dependence. A ray tracing simulation is also performed to verify the link between the observed LH emissions in the ionosphere and the HFPH wave in the magnetosphere. The remainder of this paper is organized as follows: In Section 2, we briefly introduce the DEMETER and Van Allen Probes satellites. In Section 3, we provide two event observations of LH emissions from DEMETER observations. In Section 4, we analyze and compare the wave power distributions of LH emissions and HFPH waves. Finally, a ray tracing simulation is performed in Section 5.

2. Spacecraft and Instruments

DEMETER is a French satellite with a low-altitude nearly Sun-synchronous circular orbit (∼10:30 and ∼22:30 LT). It was operated over a ∼6.5-year period from June 2004 to December 2010. The altitude of the spacecraft was initially 710 km before December 2005 and subsequently decreased to 660 km [*Parrot et al.*, 2006]. The Instrument Champ Electrique (ICE) [*Berthelier et al.*, 2006b] onboard consists of 4 sensors, which are spherical aluminum electrodes of 60 mm diameter that are deployed by stacer booms at approximately 4 m from the satellite. It can provide measurements of the electric field in the frequency range from the DC/ULF band (0-15 Hz) up to the HF band (10 kHz to 3.175 MHz). The Instrument Magnetic Search Coil (IMSC) [*Parrot et al.*, 2006] can measure the magnetic field from a few Hz to 20 kHz. The Instrument Sonde de Langmuir (ISL) is a Langmuir probe that can measure the density and temperature of electrons [*Lebreton et al.*, 2006]. The Instrument Analyseur de Plasma (IAP) is a two-analyzer spectrometer that measures the ion density, composition, temperature and flow velocity [*Berthelier et al.*, 2006a]. The background magnetic field data are calculated from the International Geomagnetic Reference Field (IGRF) 2000 model [*Olsen et al.*, 2000].

The Van Allen Probes (Van Allen Probes) [*Mauk et al.*, 2013] consist of two satellites with identical instruments with nearly similar near-equatorial highly elliptical orbits with perigees of approximately 620 km and apogees of approximately 5.8 R_E. They were launched in August 2012, and their mission ended in October 2019, with an approximately 7-year operating duration. The Waveform Receiver (WFR) of the Electric and Magnetic Field Instrument Suite and Integrated Science (EMFISIS) [*Kletzing et al.*, 2013] can provide measurements of magnetic and electric power spectral density from 10 Hz to 11.2 kHz, from which wave polarization and propagation features (such as wave normal direction, ellipticity and planarity) are calculated by the singular value decomposition (SVD) method [*Santolík et al.*, 2003]. The high-frequency receiver (HFR) can identify the upper hybrid resonance frequency between 10 and 400 kHz, which is used to calibrate the plasma density that is derived from the measurement of the spacecraft potential by the electric fields and waves (EFW) instrument [*Wygant et al.*, 2013].

3. DEMETER Observation of LH Emissions

Figure 1 shows two LH emission events that were observed by the DEMETER satellite. The first event, which occurred on January 6, 2008, is shown in Figures 1a and 1b, which present the electric field (1a) and magnetic field (Figure 1b) wave power spectral density from VLF spectra data that were measured by ICE and IMSC instruments, respectively. The white solid lines represent the value of f_{LHR} under the assumption of proton-electron plasma without heavier ions. For the f_{LHR} calculation, the magnetic field strength is obtained from the IGRF model, and the plasma density is measured by the ISL instrument of the DEMETER satellite. The ion composition measurement from the IAP instrument is subject to substantial uncertainty [*Vavilov et al.*, 2013]; thus, we did not use this ion composition for the f_{LHR} calculation. With the inclusion of additional heavy ions, f_{LHR} decreases; namely, under the assumption of proton-only plasma, the calculated f_{LHR} will overestimate the actual f_{LHR}, especially during the period when the ionospheric ion temperature is high. For higher temperatures, the ion scale height increases, and significant O^+ concentration may be expected at the DEMETER altitude. For cooler temperatures, the opposite is true, that is, H+ will be the dominant species at this altitude and thus the calculated f_{LHR} reflects the actual f_{LHR}. Consider the first event (which corresponds to the winter season for the Northern Hemisphere) in Figure 1a as an example. The satellite traveled from south to north, with magnetic latitudes varying from approximately -60° to 60°. In the region of magnetic latitude above 50°, we clearly observe strong electric emission (marked by the magenta arrows) with a lower frequency limit that well matches the pure proton f_{LHR}, which reflects the actual f_{LHR}. Over magnetic latitudes of < -50°, similar emissions are detected. However, the lower frequency limit is below and does not match the proton-only f_{LHR}, which overestimates the actual f_{LHR} in this Southern Hemisphere summer. This emission has a counterpart spectrum in the magnetic field (Figure 1b), although the wave magnetic field intensity is very weak. The second event of similar emissions, which occurred on June 2, 2010 (Northern Hemisphere summer), as shown in Figure 1c, also supports the matching of the lower frequency limit of the emissions with f_{LHR}. For the second event, the proton-only f_{LHR} reflects the actual f_{LHR} in the Southern Hemisphere while overestimating the actual f_{LHR} in the Northern Hemisphere.

Two possible sources of the LH emissions are lightning-generated whistler waves and whistler waves that are excited in the magnetosphere. To determine whether the source of the LH emissions is LGW, we examine the second event (Figure 1c), during which burst mode waveform measurements from ICE and IMSC instruments are available. The FFT power spectral density of the electric field waveform is shown in Figure 1d. The waveform spectrum shows the structure of this emission at a higher time resolution (~0.205 sec), and the time interval of the waveform spectrum is represented by the two magenta dashed lines in Figure 1c. The LH emissions are structureless and broadband. In addition to the LH emissions, we also found that lightning-generated whistler signals, which appeared as vertical strips above 5 kHz and showed frequency dispersion below 5 kHz, did not exhibit a temporal correlation with the LH emissions. Because of the differences in temporal and spectral properties, we conclude that this LH emission differs from the lightning-generated whistler waves.

4. Statistical Analysis of Data from DEMETER and the Van Allen Probes

We have presented examples of LH emissions that were observed by the DEMETER satellite. However, in a previous statistical study by *Záhlava et al.* [2018a, 2019], LH emissions (strong emissions from ∼2 kHz to ∼10 kHz in the middle latitude range) were not found in the frequency-latitude distribution of the wave power (Figure 5 in *Záhlava et al.* [2018a], Figures 2 & 3 *Záhlava et al.* [2019]). One possible reason is that in the work of *Záhlava et al.* [2018a, 2019], the statistical wave power distribution is represented by the median value, which may neglect LH emissions with stronger intensity but lower occurrence. Therefore, in this section, we replot in Figure 2 the wave power distribution by using the mean value to verify the statistical significance of the LH emissions. Figure 2a shows the mean electric wave power distribution versus frequency and magnetic latitude on the dayside, and Figure 2b shows the wave power distribution on the nightside. These wave power distributions are obtained by assigning the wave power spectra density data into bins of different frequencies and magnetic latitudes (for dayside and nightside, respectively) and calculating the mean wave power spectra density for each frequency-latitude bin. From these statistical distributions, we observe that in the middle latitude region (∼40-60°), strong emissions occur in the two hemispheres at both the dayside and nightside. The lower frequency limit decreases as the absolute latitude ($|\lambda|$) increases, which matches the variation of f_{LHR} versus the magnetic latitude. These strong emissions should be contributed mainly by the LH emissions. The emissions on the nightside in the frequency range from ∼2 kHz to ∼10 kHz over the magnetic latitude from -40° to 40° should be mainly from the LGW, which are much weaker than the LH emissions. The LGW power is much higher on the nightside than on the dayside, while in contrast, the

LH emission power is higher on the dayside. The difference in the day-night dependence further supports our previous conclusion that the LH emissions do not originate from the lightning-generated whistler.

Recently, *Maxworth et al.* [2020] reported some events from the observation of the ePOP-RRI satellite, in which there exist LH waves correlated with LGW, and they explained these LH waves are excited by the intense whistler waves. However, the LH emissions in our study do not correlate with LGW and the wave power distribution shows opposite day-night dependence compared to the distribution of LGW. Thus, we consider the source of the LH emissions in this study may be whistler waves that originate from the magnetosphere. The wave activities in the magnetosphere highly correspond to the geomagnetic activity levels; thus, we evaluate the dependence of the LH emissions on the AE index. Figures 2c and 2d show the distribution of the mean electric wave power versus frequency and the magnetic latitude on the dayside for low (<200 nT) and high (>200 nT) AE index conditions, respectively. We find that the intensity of the LH emissions is significantly higher under higher AE conditions, while the intensity of the LGW emissions in the low latitude region does not significantly depend on the AE level. This result indicates that the source of the LH emissions may be in the Earth's magnetosphere.

In the magnetosphere, a possible source of LH emissions is the high-frequency plasmaspheric hiss waves (HFPHs), which cover a similar frequency range of $\sim$ 1 kHz to >10 kHz [*He et al.*, 2019]. Using the 7-year measurements from Van Allen Probes WFR wave spectra, we perform a statistical study of the HFPH wave power distribution, which is shown in Figures 3a & b. Figure 3a and 3b show the distribution of the median magnetic field wave power of the HFPH versus frequency and the magnetic latitude of the 700 km (close to DEMETER altitude) footprints of the Van Allen Probes satellites (the corresponding dipole L shell values are also labeled) over the MLT range near 10 (9-11) hr under two AE conditions, namely, low AE (<200 nT) and high AE (>200 nT). The following filters, which are similar to those used by *He et al.* [2020], are used to extract the signals of HFPH waves: 1) Observations are made inside the plasmasphere by requiring plasma density $> 100cm^{-3}$ or $L < 2$; 2) the wave magnetic power spectral density is larger than $10^{-9}nT^2/Hz$; 3) the wave frequency ranges from 2 kHz to the lower of f_{ce} and 12 kHz (which is the upper frequency limit of the WFR instrument); 4. the wave ellipticity is larger than 0.7; and 5) the wave planarity is larger than 0.5. The wave power distribution shows strong HFPH wave power over the magnetic latitude range of the footprints from $\pm$ 55° to 65° (L shell from ~3 to 5). The frequency of the HFPH ranges from approximately 2 kHz to 12 kHz, and the frequency increases as the absolute value of the magnetic latitude decreases. The frequency range of the HFPH waves is close to that of the LH emissions that were observed by the DEMETER satellite. The dependence of the wave frequency on the magnetic latitude is consistent between the two types of emissions. The footprint latitude range of the HFPH waves, although slightly narrower, is close to that of the LH emissions. This slight discrepancy in the latitude range may be explained by the oblique propagation of the whistler waves. The HFPH wave power is higher under the higher AE condition, which is consistent with that for the LH emissions. From the results in Figure 2 of *He et al.* [2020], the HFPH on the dayside wave power is higher than that on the nightside, which is also in agreement with the dependence of the LH waves on the local time. In summary, the statistical study of the wave power distributions of LH and HFPH waves shows similar frequency ranges and magnetic latitude ranges, along with consistent AE dependence and MLT dependence. Such common properties support that the LH emissions originate from the HFPH waves in the magnetosphere.

Using the same Van Allen Probes WFR data, we examine the HFPH wave normal angle distribution on the meridional plane for a selected frequency of 4 kHz, which is shown in Figure 3c. The result shows that at $L > 3$, the median HFPH wave normal angles are quasi-parallel and anti-parallel to the background magnetic field in the Northern and Southern Hemispheres, respectively. This wave normal distribution suggests that the HFPH propagates away from the equatorial source in the magnetosphere, which is consistent with our conclusion that the HFPH is the source of the LH emissions in the ionosphere.

5. Ray Tracing Simulation Results

In the previous section, we showed observationally that the LH emissions in the ionosphere originate from HFPH waves in the inner magnetosphere. To verify this hypothesis, we run a ray tracing simulation to check whether HFPH waves can propagate down toward low altitudes and are limited above f_{LHR}. We use the HOTRAY ray tracing code [*Horne*, 1989] with a dipole magnetic field and a diffusive equilibrium plasma density model [*Bortnik et al.*, 2011, and references within]. The density model has implemented a much-simplified density component in the ionosphere (see the details in *Bortnik et al.* [2011]), which performs adequately for our purpose of testing the hypothesis. To more accurately model the LH emission spectra, a realistic ionospheric model (such as the international reference ionosphere [*Bilitza et al.*, 2017; *Bilitza*, 2018]) may be used, which is beyond the scope of this study.

In the ray tracing simulation, waves with frequencies from 6 to 14 kHz are launched at the equator at L = 3.75 with an initial wave normal angle of 0°. The results of the ray tracing simulation are shown in Figure 4. Figure 4a shows the distribution of background plasma density in the meridional plane and Figure 4b shows the distribution of the local f_{LHR}. Figure 4c shows the ray paths for waves with various frequencies (colored solid lines), Figures 4d and 4e show the variation of magnetic latitude and local f_{LHR} for ray paths. From the f_{LHR} distribution (Figure 4b), we observe that f_{LHR} reaches its maximum value (∼10 kHz) near the topside of the ionosphere, and the peak is formed because f_{LHR} value increases with magnetic field but decreases with plasma density especially at low altitudes. Initially, the waves can propagate nearly along the magnetic field into the ionosphere. The paths of higher frequency rays bend inward and can reach the ionospheric altitude at a smaller value of L. After reaching the ionosphere, the rays with frequencies that are lower than 10 kHz are reflected, propagate back to the equator and then to the Southern Hemisphere (Figure 4c). From Figure 4e, we can see that as the rays initially propagate to higher latitudes, f_{LHR} increases due to the increasing background magnetic field. When the wave frequency falls just below the local f_{LHR}, the waves are reflected. For example, the low frequency wave (6 kHz, cyan line) is reflected at higher altitude than the high frequency wave (8 kHz, green line) since the local f_{LHR} values increase during the propagation away from the equator. This reflection is also known as magnetospheric reflection, although it can occur near the ionospheric altitude. Because of the magnetospheric reflection, at a fixed ionospheric location, only waves with frequencies that exceed the local f_{LHR} can access and thus be observed. Our model also includes the effect of Landau Damping and the variation of wave power gain is shown in Figure 4f. We can see that when the waves reach the topside of the ionosphere, the wave damping is less than -10 dB for all the rays and the waves are still strong enough to be observed. This ray tracing simulation demonstrates the physical feasibility of HFPH waves accessing ionospheric altitudes, and magnetospheric reflection just below f_{LHR} may explain the observed LH emission spectrum with a lower frequency limit near f_{LHR}.

6. Conclusions and Discussion

Using the 6.5-year observation data of the DEMETER satellite, we present the LH emission, which is a type of strong electromagnetic emission with a lower frequency limit that is near the local f_{LHR}. We perform a statistical study on the distribution of the wave power versus the frequency, geomagnetic latitude, MLT and AE index for the LH emissions. Additionally, we perform a statistical study on their counterparts in the magnetosphere, namely, HFPH waves. A ray tracing simulation is carried out to test the physical connection between the two types of emissions. The features of the LH emissions are summarized as follows:

1. The LH emissions have structureless spectra with distinct lower frequency limits that are near f_{LHR} and occur in the latitude ranges of 40° to 60° in the Northern Hemisphere and -40° to -60° in the Southern Hemisphere.

2. The lower frequency limit of the LH emissions increases as the absolute value of the geomagnetic latitude decreases, which follows the latitudinal variation of f_{LHR}.

3. The intensity of the LH emissions is stronger on the dayside (MLT ∼10) and under higher AE conditions.

Given the above properties of the LH emissions, we exclude the LGW as the source of the LH emissions and identify the HFPH as the most likely source. We compare the statistical properties of the LH waves from the DEMETER observations and the HFPH emissions from the Van Allen Probes observations. The comparison shows similarities in the frequency range and the invariant magnetic latitude range and shows consistent dependences on MLT and the AE index. Furthermore, the distribution of HFPH wave normals shows that the HFPH propagates away from the equator in the magnetosphere, which further supports that the observed LH emissions at the topside of the ionosphere are caused by the HFPH waves propagating into the ionosphere. Finally, we perform a ray tracing simulation and demonstrate the process by which whistler waves propagate from the equator to the ionospheric altitude. The process of magnetospheric reflection occurs when the wave frequency falls just below the local f_{LHR}, which explains the observed lower frequency limit of the LH emissions near f_{LHR}. Recent study [*Meredith et al.*, 2021] suggests that the HFPH observed in *He et al.* [2019, 2020] should be the chorus waves outside the plasmapause. The HFPH in *He et al.* [2019, 2020] and in our study, however, are confirmed inside the high-density plasmasphere by requiring that the plasma density exceeeds a critical value (100 cm^{-3} in this study), the observed HFPH is unlikely the chorus waves, which are observed in the low density plamsa trough region.

In addition to the LGW, we also exclude auroral hiss as a potential source of LH emissions. The auroral hiss occurs over a wide frequency range from a few hundred Hz to several tens of kHz and is often observed by the in-situ satellite with a "funnel-shaped" frequency-time signature, which is caused by the narrow latitudinal range (5-10° near the auroral zone) for the low-frequency band and the wider range for the high-frequency band [*Smith*, 1969; *Mosier and Gurnett*, 1969; *James*, 1976]. The auroral hiss is suggested to be produced by electron beams that are associated with the aurora in the high-latitude magnetosphere [*Maggs*, 1976; *Pfaff et al.*, 2001; *Ergun et al.*, 2003; *Kopf et al.*, 2010]. We find that the auroral hiss is unlikely to be the source of the LH emissions for the following reasons. 1. The auroral hiss can be observed only inside or near the auroral zones, which are at higher latitudes than the LH emissions. 2. The in-situ observed spectra of the auroral hiss exhibit a funnel-shaped frequency-time structure, while the LH emission spectra do not. 3. The occurrence and amplitude of the auroral hiss increase on the nightside, compared to the dayside [*Spasojevic*, 2016]. This local time dependence is opposite to that of the LH emission wave. 4. The auroral hiss propagates upwards and away from the Earth, so it won't be able to get down to the low altitude of the DEMETER orbit.

Using the detected LH emission spectra with the lower frequency limit being f_{LHR}, we can roughly estimate the proportion of heavy ions at the topside of the ionosphere. The supplemental material briefly introduces how to estimate the O^+ composition in the ions from the LH emission spectra under the assumption that the ions only contain protons and O^+.

Acknowledgments. The work at UTD was supported by NASA grants 80NSSC19K0282, 80NSSC20K1324, 80NSSC21K1688, and 80NSSC21K0728. RH was supported by NERC

Highlight Topic Grant NE/P01738X/1 (Rad-Sat) and NERC grant NE/V00249X/1 (Sat-Risk). This study is related to data that was recorded by the DEMETER microsatellite, which was operated thanks to the French Centre National D'Etudes Spatiales (CNES). We also thank J.J. Berthelier and J.P. Lebreton, who are the PIs of ICE and ISL, respectively. The DEMETER data that are presented in the paper can be downloaded from https://cdpp-archive.cnes.fr/. The Van Allen Probes data can be downloaded from SPDF https://spdf.gsfc.nasa.gov/pub/data/rbsp/.

References

Artemyev, A. V., A. A. Vasiliev, D. Mourenas, O. V. Agapitov, and V. V. Krasnoselskikh (2013), Nonlinear electron acceleration by oblique whistler waves: Landau resonance vs. cyclotron resonance, *Physics of Plasmas*, *20*(12), 122,901, doi:10.1063/1.4836595.

Bell, T. F. (1984), The nonlinear gyroresonance interaction between energetic electrons and coherent vlf waves propagating at an arbitrary angle with respect to the earth's magnetic field, *Journal of Geophysical Research: Space Physics*, *89*(A2), 905–918, doi: https://doi.org/10.1029/JA089iA02p00905.

Bell, T. F. (1986), The wave magnetic field amplitude threshold for nonlinear trapping of energetic gyroresonant and landau resonant electrons by nonducted vlf waves in the magnetosphere, *Journal of Geophysical Research: Space Physics*, *91*(A4), 4365–4379, doi:https://doi.org/10.1029/JA091iA04p04365.

Berthelier, J., M. Godefroy, F. Leblanc, M. Malingre, M. Menvielle, D. Lagoutte, J. Brochot, F. Colin, F. Elie, C. Legendre, P. Zamora, D. Benoist, Y. Chapuis, J. Artru, and R. Pfaff (2006a), Ice, the electric field experiment on demeter, *Planetary and Space*

Science, *54*(5), 456 – 471, doi:https://doi.org/10.1016/j.pss.2005.10.016, first Results of the DEMETER Micro-Satellite.

Berthelier, J. J., M. Godefroy, F. Leblanc, M. Malingre, M. Menvielle, D. Lagoutte, J. Y. Brochot, F. Colin, F. Elie, C. Legendre, P. Zamora, D. Benoist, Y. Chapuis, J. Artru, and R. Pfaff (2006b), ICE, the electric field experiment on DEMETER, *Planetary and Space Science*, *54*(5), 456–471, doi:https://doi.org/10.1016/j.pss.2005.10.016.

Bilitza, D. (2018), IRI the International Standard for the Ionosphere, *Advances in Radio Science*, *16*, 1–11, doi:10.5194/ars-16-1-2018.

Bilitza, D., D. Altadill, V. Truhlik, V. Shubin, I. Galkin, B. Reinisch, and X. Huang (2017), International reference ionosphere 2016: From ionospheric climate to real-time weather predictions, *Space Weather*, *15*(2), 418–429, doi: https://doi.org/10.1002/2016SW001593.

Bortnik, J., U. S. Inan, and T. F. Bell (2003), Energy distribution and lifetime of magnetospherically reflecting whistlers in the plasmasphere, *Journal of Geophysical Research: Space Physics*, *108*(A5), doi:https://doi.org/10.1029/2002JA009316.

Bortnik, J., R. M Thorne, and N. Meredith (2008), The unexpected origin of plasmaspheric hiss from discrete chorus waves, *Nature*, *452*, 62–66, doi:10.1038/nature06741.

Bortnik, J., R. M. Thorne, and N. P. Meredith (2009), Plasmaspheric hiss overview and relation to chorus, *Journal of Atmospheric and Solar-Terrestrial Physics*, *71*(16), 1636–1646, doi:https://doi.org/10.1016/j.jastp.2009.03.023.

Bortnik, J., L. Chen, W. Li, R. M. Thorne, and R. B. Horne (2011), Modeling the evolution of chorus waves into plasmaspheric hiss, *Journal of Geophysical Research:*

Space Physics, *116* (A8), doi:10.1029/2011JA016499.

Chen, L., J. Bortnik, R. M. Thorne, R. B. Horne, and V. K. Jordanova (2009), Three-dimensional ray tracing of VLF waves in a magnetospheric environment containing a plasmaspheric plume, *Geophysical Research Letters*, *36* (22), doi:10.1029/2009GL040451.

Chen, L., J. Bortnik, W. Li, R. M. Thorne, and R. B. Horne (2012), Modeling the properties of plasmaspheric hiss: 1. dependence on chorus wave emission, *Journal of Geophysical Research: Space Physics*, *117* (A5), doi:https://doi.org/10.1029/2011JA017201.

Chum, J., and O. Santolík (2005), Propagation of whistler-mode chorus to low altitudes: divergent ray trajectories and ground accessibility, *Annales Geophysicae*, *23* (12), 3727–3738, doi:10.5194/angeo-23-3727-2005.

Draganov, A. B., U. S. Inan, V. S. Sonwalkar, and T. F. Bell (1992), Magnetospherically reflected whistlers as a source of plasmaspheric hiss, *Geophysical Research Letters*, *19* (3), 233–236, doi:https://doi.org/10.1029/91GL03167.

Ergun, R. E., C. W. Carlson, J. P. McFadden, R. J. Strangeway, M. V. Goldman, and D. L. Newman (2003), Fast auroral snapshot satellite observations of very low frequency saucers, *Physics of Plasmas*, *10* (2), 454–462, doi:10.1063/1.1530160.

Green, A., W. Li, Q. Ma, X.-C. Shen, J. Bortnik, and G. B. Hospodarsky (2020), Properties of lightning generated whistlers based on van allen probes observations and their global effects on radiation belt electron loss, *Geophysical Research Letters*, *47* (17), e2020GL089,584, doi:https://doi.org/10.1029/2020GL089584, e2020GL089584 2020GL089584.

He, Z., L. Chen, X. Liu, H. Zhu, S. Liu, Z. Gao, and Y. Cao (2019), Local generation of high-frequency plasmaspheric hiss observed by van allen probes, *Geophysical Research Letters*, *46*(3), 1141–1148, doi:https://doi.org/10.1029/2018GL081578.

He, Z., J. Yu, L. Chen, Z. Xia, W. Wang, K. Li, and J. Cui (2020), Statistical study on locally generated high-frequency plasmaspheric hiss and its effect on suprathermal electrons: Van allen probes observation and quasi-linear simulation, *Journal of Geophysical Research: Space Physics*, *125*(10), e2020JA028,526, doi: https://doi.org/10.1029/2020JA028526, e2020JA028526 10.1029/2020JA028526.

Horne, R. B. (1989), Path-integrated growth of electrostatic waves: The generation of terrestrial myriametric radiation, *Journal of Geophysical Research: Space Physics*, *94*(A7), 8895–8909, doi:10.1029/JA094iA07p08895.

Inan, U. S., and T. F. Bell (1991), Pitch angle scattering of energetic particles by oblique whistler waves, *Geophysical Research Letters*, *18*(1), 49–52, doi: https://doi.org/10.1029/90GL02476.

Inan, U. S., and S. Tkalcevic (1982), Nonlinear equations of motion for landau resonance interactions with a whistler mode wave, *Journal of Geophysical Research: Space Physics*, *87*(A4), 2363–2367, doi:https://doi.org/10.1029/JA087iA04p02363.

James, H. G. (1976), Vlf saucers, *Journal of Geophysical Research (1896-1977)*, *81*(4), 501–514, doi:https://doi.org/10.1029/JA081i004p00501.

Jiřiček, F., D. R. Shklyar, and P. Třiska (2001), Lhr effects in nonducted whistler propagation – new observations and numerical modelling, *Annales Geophysicae*, *19*(2), 147–157, doi:10.5194/angeo-19-147-2001.

Kletzing, C. A., W. S. Kurth, M. Acuna, R. J. MacDowall, R. B. Torbert, T. Averkamp, D. Bodet, S. R. Bounds, M. Chutter, J. Connerney, D. Crawford, J. S. Dolan, R. Dvorsky, G. B. Hospodarsky, J. Howard, V. Jordanova, R. A. Johnson, D. L. Kirchner, B. Mokrzycki, G. Needell, J. Odom, D. Mark, R. Pfaff, J. R. Phillips, C. W. Piker, S. L. Remington, D. Rowland, O. Santolik, R. Schnurr, D. Sheppard, C. W. Smith, R. M. Thorne, and J. Tyler (2013), The Electric and Magnetic Field Instrument Suite and Integrated Science (EMFISIS) on RBSP, *Space Sci Rev*, *179*, 127–181, doi:10.1007/s11214-013-9993-6.

Kopf, A. J., D. A. Gurnett, J. D. Menietti, P. Schippers, C. S. Arridge, G. B. Hospodarsky, W. S. Kurth, S. Grimald, N. André, A. J. Coates, and M. K. Dougherty (2010), Electron beams as the source of whistler-mode auroral hiss at saturn, *Geophysical Research Letters*, *37*(9), doi:https://doi.org/10.1029/2010GL042980.

Lebreton, J.-P., S. Stverak, P. Travnicek, M. Maksimovic, D. Klinge, S. Merikallio, D. Lagoutte, B. Poirier, P.-L. Blelly, Z. Kozacek, and M. Salaquarda (2006), The isl langmuir probe experiment processing onboard demeter: Scientific objectives, description and first results, *Planetary and Space Science*, *54*(5), 472 – 486, doi:https://doi.org/10.1016/j.pss.2005.10.017, first Results of the DEMETER Micro-Satellite.

Li, W., R. M. Thorne, J. Bortnik, G. D. Reeves, C. A. Kletzing, W. S. Kurth, G. B. Hospodarsky, H. E. Spence, J. B. Blake, J. F. Fennell, S. G. Claudepierre, J. R. Wygant, and S. A. Thaller (2013), An unusual enhancement of low-frequency plasmaspheric hiss in the outer plasmasphere associated with substorm-injected electrons, *Geophysical*

Research Letters, *40*(15), 3798–3803, doi:10.1002/grl.50787.

Lyons, L., and R. Thorne (1970), The magnetospheric reflection of whistlers, *Planetary and Space Science*, *18*(12), 1753–1767, doi:https://doi.org/10.1016/0032-0633(70)90009-7.

Maggs, J. E. (1976), coherent generation of vlf hiss, *Journal of Geophysical Research (1896-1977)*, *81*(10), 1707–1724, doi:https://doi.org/10.1029/JA081i010p01707.

Mauk, B. H., N. J. Fox, S. G. Kanekal, R. L. Kessel, D. G. Sibeck, and A. Ukhorskiy (2013), Science Objectives and Rationale for the Radiation Belt Storm Probes Mission, *Space Sci Rev*, *179*(1-4), 3–27, doi:10.1007/s11214-012-9908-y.

Maxworth, A., G. Hussey, and M. Gokowski (2020), Coexistence of lightning generated whistlers, hiss and lower hybrid noise observed by e-pop (swarm-e)rri, *Atmosphere*, *11*(2), doi:10.3390/atmos11020177.

Meredith, N. P., R. B. Horne, M. A. Clilverd, D. Horsfall, R. M. Thorne, and R. R. Anderson (2006), Origins of plasmaspheric hiss, *Journal of Geophysical Research: Space Physics*, *111*(A9), doi:10.1029/2006JA011707.

Meredith, N. P., J. Bortnik, R. B. Horne, W. Li, and X.-C. Shen (2021), Statistical investigation of the frequency dependence of the chorus source mechanism of plasmaspheric hiss, *Geophysical Research Letters*, *48*(6), e2021GL092,725, doi: https://doi.org/10.1029/2021GL092725, e2021GL092725 2021GL092725.

Mosier, S. R., and D. A. Gurnett (1969), Vlf measurements of the poynting flux along the geomagnetic field with the injun 5 satellite, *Journal of Geophysical Research (1896-1977)*, *74*(24), 5675–5687, doi:https://doi.org/10.1029/JA074i024p05675.

Němec, F., O. Santolík, M. Parrot, and C. J. Rodger (2010), Relationship between median intensities of electromagnetic emissions in the vlf range and lightning activity, *Journal of Geophysical Research: Space Physics*, *115*(A8), doi: https://doi.org/10.1029/2010JA015296.

Ni, B., J. Bortnik, R. M. Thorne, Q. Ma, and L. Chen (2013), Resonant scattering and resultant pitch angle evolution of relativistic electrons by plasmaspheric hiss, *Journal of Geophysical Research: Space Physics*, *118*(12), 7740–7751, doi: https://doi.org/10.1002/2013JA019260.

Ni, B., W. Li, R. M. Thorne, J. Bortnik, Q. Ma, L. Chen, C. A. Kletzing, W. S. Kurth, G. B. Hospodarsky, G. D. Reeves, H. E. Spence, J. Bernard Blake, J. F. Fennell, and S. G. Claudepierre (2014), Resonant scattering of energetic electrons by unusual low-frequency hiss, *Geophysical Research Letters*, *41*(6), 1854–1861, doi: https://doi.org/10.1002/2014GL059389.

Olsen, N., T. J. Sabaka, and L. Tøffner-Clausen (2000), Determination of the IGRF 2000 model, *Earth, Planets and Space*, *52*, 1175–1182, doi:10.1186/BF03352349.

Parrot, M., D. Benoist, J. Berthelier, J. Becki, Y. Chapuis, F. Colin, F. Elie, P. Fergeau, D. Lagoutte, F. Lefeuvre, C. Legendre, M. Lvque, J. Pinon, B. Poirier, H.-C. Seran, and P. Zamora (2006), The magnetic field experiment imsc and its data processing onboard demeter: Scientific objectives, description and first results, *Planetary and Space Science*, *54*(5), 441–455, doi:https://doi.org/10.1016/j.pss.2005.10.015, first Results of the DEMETER Micro-Satellite.

Pfaff, R., C. Carlson, J. Watzin, D. Everett, and T. Gruner (2001), An overview of the fast auroral snapshot (fast) satellite, *Space Science Reviews*, *98*(1), 1–32, doi: 10.1023/A:1013187826070.

Ripoll, J.-F., T. Farges, D. M. Malaspina, E. H. Lay, G. S. Cunningham, G. B. Hospodarsky, C. A. Kletzing, and J. R. Wygant (2020), Analysis of electric and magnetic lightning-generated wave amplitudes measured by the van allen probes, *Geophysical Research Letters*, *47*(6), e2020GL087,503, doi:https://doi.org/10.1029/2020GL087503, e2020GL087503 2020GL087503.

Santolík, O., D. A. Gurnett, J. S. Pickett, M. Parrot, and N. Cornilleau-Wehrlin (2003), Spatio-temporal structure of storm-time chorus, *Journal of Geophysical Research: Space Physics*, *108*(A7), doi:10.1029/2002JA009791.

Shi, R., W. Li, Q. Ma, G. D. Reeves, C. A. Kletzing, W. S. Kurth, G. B. Hospodarsky, H. E. Spence, J. B. Blake, J. F. Fennell, and S. G. Claudepierre (2017), Systematic evaluation of low-frequency hiss and energetic electron injections, *Journal of Geophysical Research: Space Physics*, *122*(10), 10,263–10,274, doi: https://doi.org/10.1002/2017JA024571.

Shklyar, D., and H. Matsumoto (2009), Oblique whistler-mode waves in the inhomogeneous magnetospheric plasma: Resonant interactions with energetic charged particles, *Surveys in Geophysics*, *30*(2), 55–104, doi:10.1007/s10712-009-9061-7.

Shklyar, D. R., J. Chum, and F. Jiříček (2004), Characteristic properties of nu whistlers as inferred from observations and numerical modelling, *Annales Geophysicae*, *22*(10), 3589–3606, doi:10.5194/angeo-22-3589-2004.

Smith, R. L. (1969), Vlf observations of auroral beams as sources of a class of emissions, *Nature*, *224*(5217), 351–352, doi:10.1038/224351a0.

Sonwalkar, V., and U. Inan (1989), Lightning as an embryonic source of VLF hiss, *J. Geophys. Res.,* , *94*, 6986–6994, doi:10.1029/JA094iA06p06986.

Spasojevic, M. (2016), Statistics of auroral hiss and relationship to auroral boundaries and upward current regions, *Journal of Geophysical Research: Space Physics*, *121*(8), 7547–7560, doi:https://doi.org/10.1002/2016JA022851.

Su, Z., N. Liu, H. Zheng, Y. Wang, and S. Wang (2018), Large-amplitude extremely low frequency hiss waves in plasmaspheric plumes, *Geophysical Research Letters*, *45*(2), 565–577, doi:https://doi.org/10.1002/2017GL076754.

Thorne, R. M., E. J. Smith, R. K. Burton, and R. E. Holzer (1973), Plasmaspheric hiss, *Journal of Geophysical Research (1896-1977)*, *78*(10), 1581–1596, doi:10.1029/JA078i010p01581.

Vavilov, D., D. Shklyar, E. Titova, and M. Parrot (2013), Study of the lower hybrid resonance frequency over the regions of gathering earthquakes using demeter data, *Journal of Atmospheric and Solar-Terrestrial Physics*, *100-101*, 1–12, doi:https://doi.org/10.1016/j.jastp.2013.03.019.

Wygant, J. R., J. W. Bonnell, K. Goetz, R. E. Ergun, F. S. Mozer, S. D. Bale, M. Ludlam, P. Turin, P. R. Harvey, R. Hochmann, K. Harps, G. Dalton, J. McCauley, W. Rachelson, D. Gordon, B. Donakowski, C. Shultz, C. Smith, M. Diaz-Aguado, J. Fischer, S. Heavner, P. Berg, D. M. Malsapina, M. K. Bolton, M. Hudson, R. J. Strangeway, D. N. Baker, X. Li, J. Albert, J. C. Foster, C. C. Chaston, I. Mann, E. Donovan, C. M.

Cully, C. A. Cattell, V. Krasnoselskikh, K. Kersten, A. Brenneman, and J. B. Tao (2013), The Electric Field and Waves Instruments on the Radiation Belt Storm Probes Mission, *Space Sci Rev*, *179*(1-4), 183–220, doi:10.1007/s11214-013-0013-7.

Xu, X., L. Chen, C. Zhou, X. Liu, Z. Xia, J. J. Simpson, and Y. Zhang (2020), Two-dimensional full-wave simulation of whistler mode wave propagation near the local lower hybrid resonance frequency in a dipole field, *Journal of Geophysical Research: Space Physics*, *125*(4), e2019JA027,750, doi:https://doi.org/10.1029/2019JA027750, e2019JA027750 2019JA027750.

Yu, J., L. Y. Li, J. B. Cao, L. Chen, J. Wang, and J. Yang (2017), Propagation characteristics of plasmaspheric hiss: Van allen probe observations and global empirical models, *Journal of Geophysical Research: Space Physics*, *122*(4), 4156–4167, doi:https://doi.org/10.1002/2016JA023372.

Yue, C., L. Chen, J. Bortnik, Q. Ma, R. M. Thorne, V. Angelopoulos, J. Li, X. An, C. Zhou, C. Kletzing, G. D. Reeves, and H. E. Spence (2017), The characteristic response of whistler mode waves to interplanetary shocks, *Journal of Geophysical Research: Space Physics*, *122*(10), 10,047–10,057, doi: https://doi.org/10.1002/2017JA024574.

Záhlava, J., F. Němec, J. L. Pincon, O. Santolík, I. Kolmašová, and M. Parrot (2018a), Whistler influence on the overall very low frequency wave intensity in the upper ionosphere, *Journal of Geophysical Research: Space Physics*, *123*(7), 5648–5660, doi: https://doi.org/10.1029/2017JA025137.

Záhlava, J., F. Němec, O. Santolík, I. Kolmašova, G. B. Hospodarsky, M. Parrot, W. S. Kurth, J. Bortnik, and C. Kletzing (2018b), Longitudinal dependence of whistler mode electromagnetic waves in the earth's inner magnetosphere, *Journal of Geophysical Research: Space Physics*, *123*(8), 6562–6575, doi:https://doi.org/10.1029/2018JA025284.

Záhlava, J., F. Němec, O. Santolík, I. Kolmašová, G. B. Hospodarsky, M. Parrot, W. S. Kurth, and C. A. Kletzing (2019), Lightning contribution to overall whistler mode wave intensities in the plasmasphere, *Geophysical Research Letters*, *46*(15), 8607–8616, doi:https://doi.org/10.1029/2019GL083918.

Zheng, H., R. H. Holzworth, J. B. Brundell, A. R. Jacobson, J. R. Wygant, G. B. Hospodarsky, F. S. Mozer, and J. Bonnell (2016), A statistical study of whistler waves observed by van allen probes (rbsp) and lightning detected by wwlln, *Journal of Geophysical Research: Space Physics*, *121*(3), 2067–2079, doi:https://doi.org/10.1002/2015JA022010.

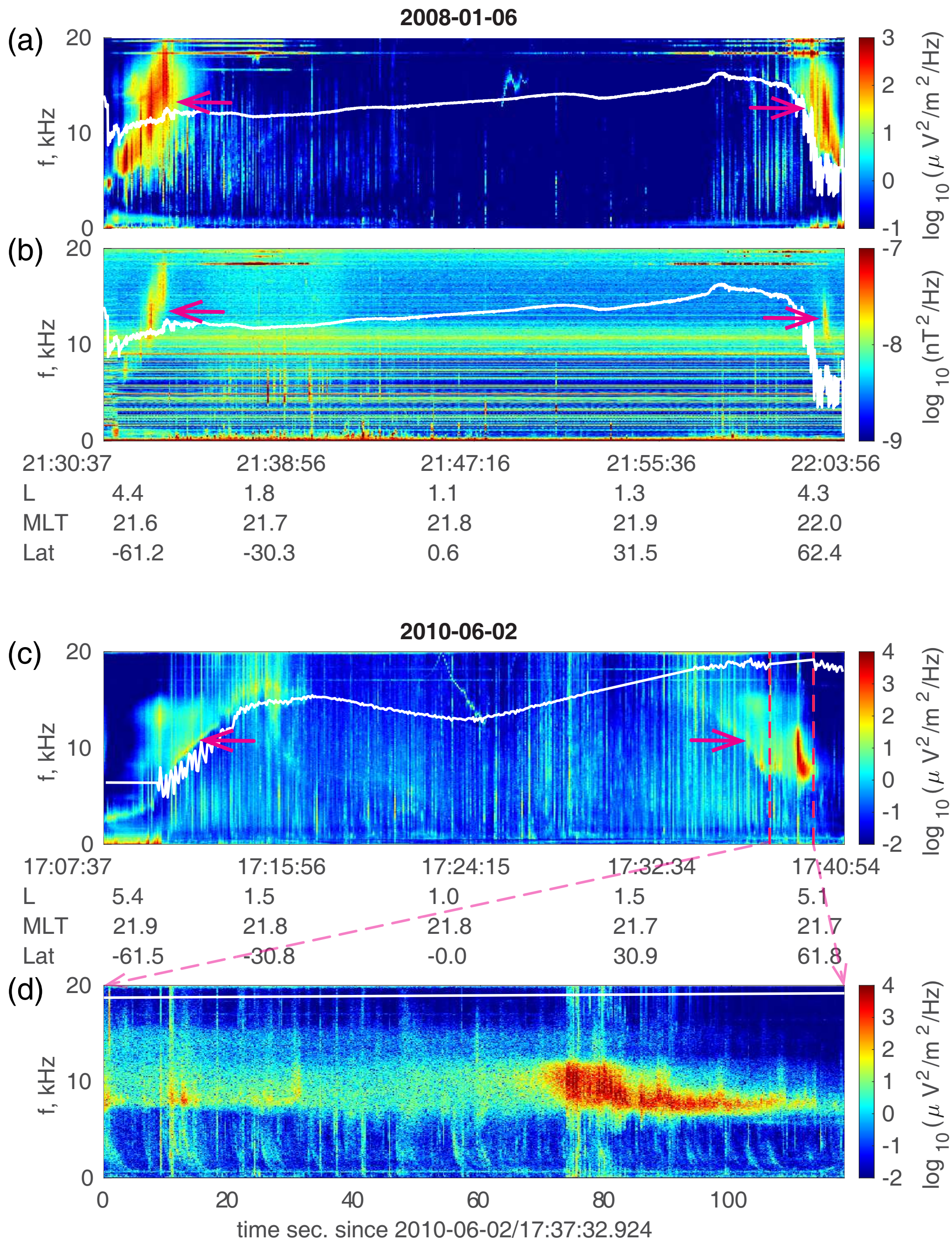

Figure 1. Two events of LH emissions that were observed by the DEMETER satellite. (a) and (b) show the electric field and magnetic field wave spectra of the first event. (c) shows the electric field spectrum for the second event. (d) shows the FFT spectra of the electric field waveform data for the time interval labeled by the two magenta dashed lines in the second event. The white solid lines represent the variation of the pure proton f_{LHR}. The magenta arrows point to the LH emissions.

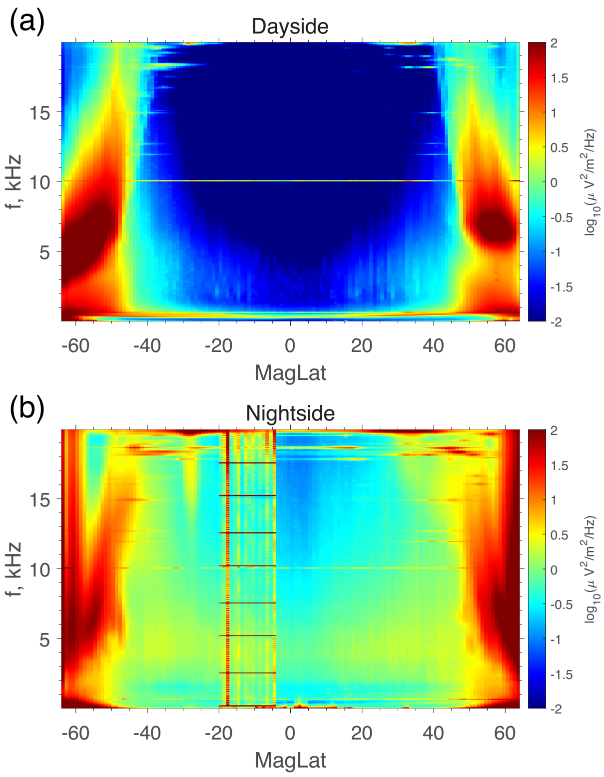

Figure 2. Mean electric wave power distribution versus frequency (y-axis) and magnetic latitude (x-axis) from the DEMETER observations for the dayside (a) and nightside (b), and for low AE (<200 nT) condition (c) and high AE (>200 nT) condition (d) on the dayside.

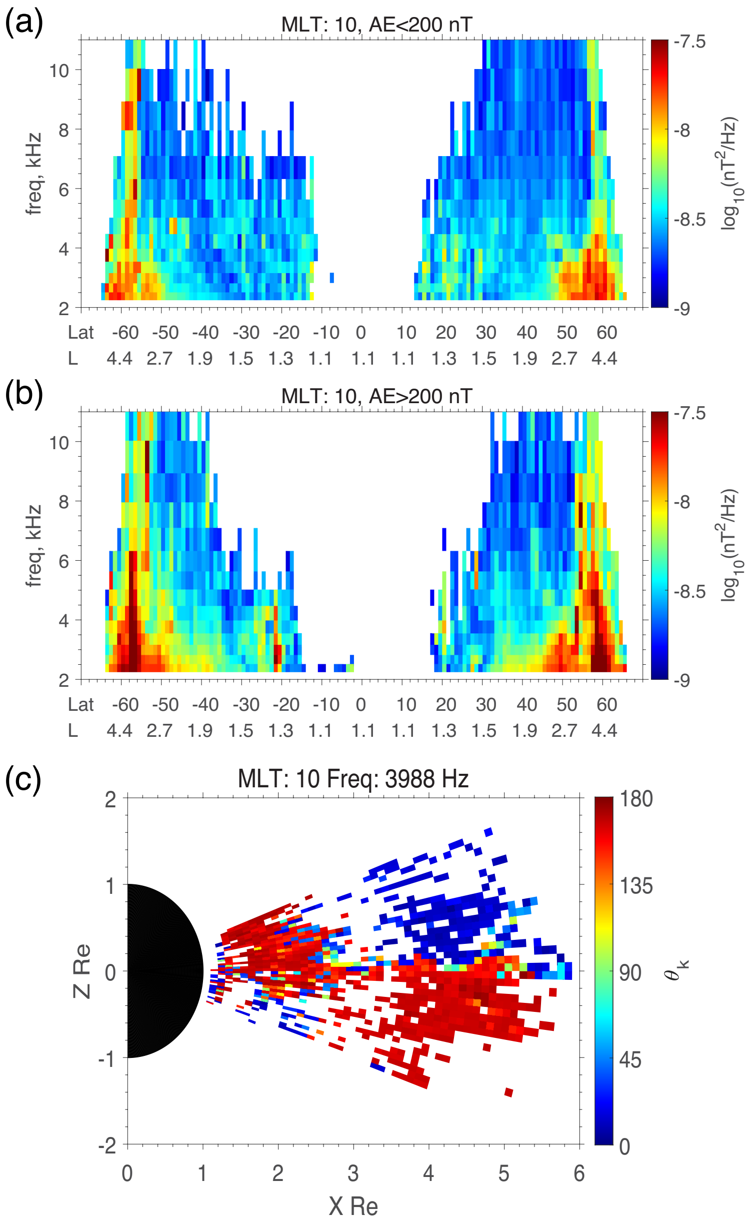

Figure 3. Median magnetic wave power distribution versus frequency (y-axis) and magnetic latitude of the 700km footprints and the corresponding dipole L shell (x-axis) from the Van Allen Probes observations on the dayside (MLT near 10) for low AE (<200 nT) condition (c) and high AE (>200 nT) condition (b). (c) is the meridional distribution of the median wave normal angle for a 3988 Hz wave.

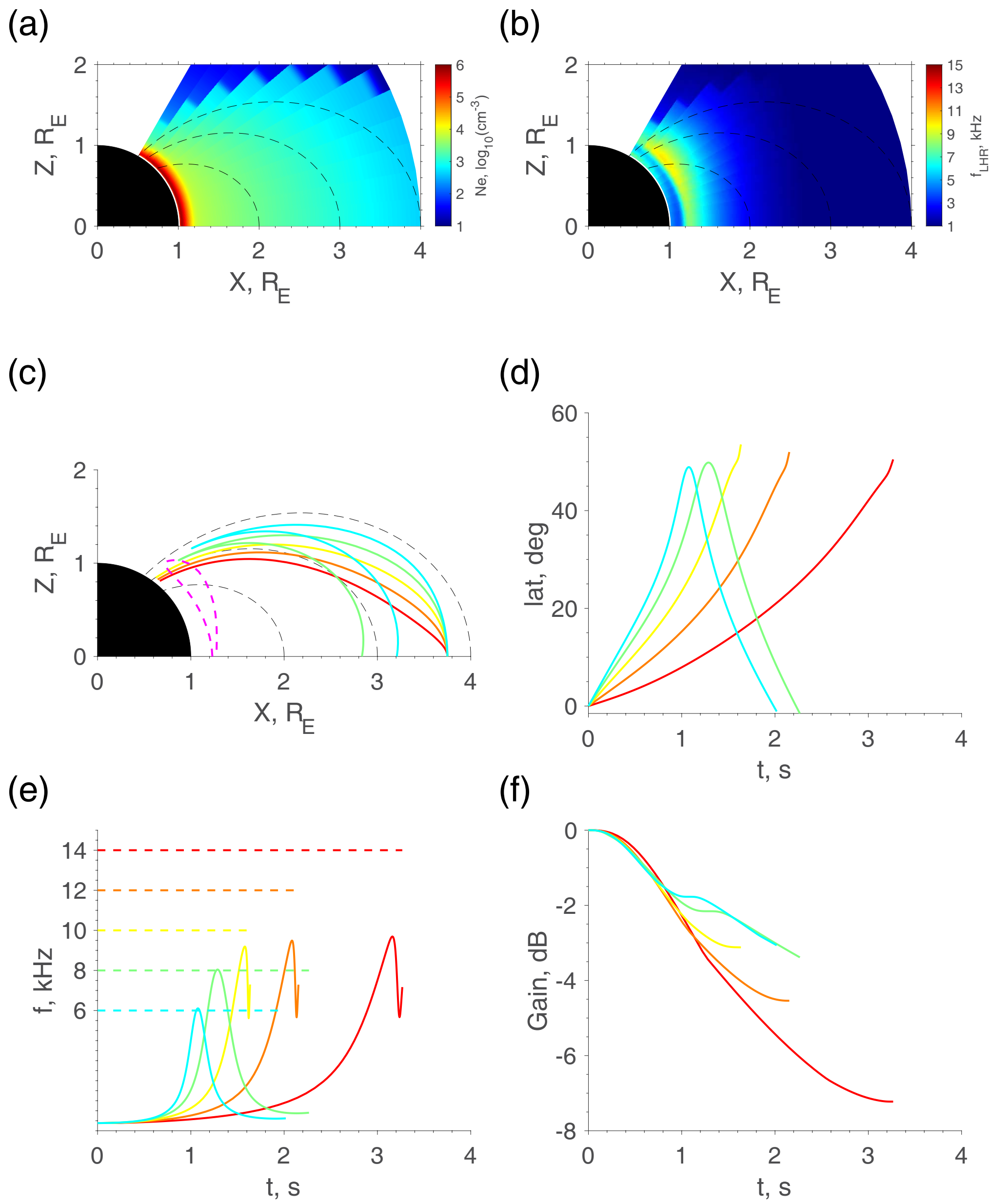

Figure 4. Ray tracing simulation results for waves that are launched at the equator and L=3.75 with frequencies from 6 to 14 kHz. (a) the distribution of the plasma density. (b) the distribution of the local f_{LHR}. (c) the ray paths of waves of different frequencies. (d) the variation of the rays' magnetic latitude, (e) the variation of the local f_{LHR} (solid lines) along the ray paths, with wave frequency also shown by dashed lines as comparison. (f) the variation of the path-integrated wave gain along the ray paths. A contour of f_{LHR}=8 kHz is overplotted as the magenta dashed line in (c).